Illumination and fluorescence collection volumes for fiber optic probes in tissue

Dean C.S. Tai
The University of Auckland
Bioengineering Institute and
Department of Physics
Auckland, New Zealand 1001

Darren A. Hooks
The University of Auckland
Bioengineering Institute and
Department of Physiology
Auckland, New Zealand 1001

John D. Harvey
The University of Auckland
Department of Physics
Auckland, New Zealand 1001

Bruce H. Smaill
The University of Auckland
Bioengineering Institute and
Department of Physiology
Auckland, New Zealand 1001

Christian Soeller
The University of Auckland
Department of Physiology
Auckland, New Zealand 1001

Abstract. Optical fibers can deliver light to, and collect it from, regions deep in tissue. However, reported illumination and fluorescence collection volumes adjacent to the fiber tip have been inconsistent, and systematic data on this topic are not available. Illumination and fluorescence collection profiles were characterized with high spatial resolution for different optical fibers in tissue and various fluids using two-photon flash photolysis and excitation. We confirm that illumination and fluorescence collection volumes for optical fibers are near identical. Collection volume is determined by the core dimensions and numerical aperture (NA) of the fiber and the scattering properties of the medium. For a multimode optical fiber with 100 μm core diam and NA=0.22, 80% of the total fluorescence is collected from a depth of 170 μm in tissue and 465 μm in nonscattering fluid. A semiempirical mathematical description of photon flux adjacent to the fiber tip was also developed and validated. This was used to quantify the extent of temporal blurring associated with propagation of a wavefront of altered fluorescence emission across the region addressed by fiber optic probes. We provide information that will facilitate the design of optical probes for tissue imaging or therapeutic applications.
 [DOI: 10.1117/1.2750288]

Keywords: fluorescence imaging; optical probe; imaging system; collection volume; illumination volume; intramural measurement.

Paper 06227R received Aug. 22, 2006; revised manuscript received Jan. 23, 2007; accepted for publication Jan. 23, 2007; published online Jun. 28, 2007.

1 Introduction

Over the past two decades, optical fibers have been employed in biophotonics applications in a variety of novel ways. Fiber-based measurement of fluorescence from functional dyes has yielded important information about biological processes and pathology. For instance, optical fibers have been employed in the detection of subsurface tumors in rat models.[1] Recently, a new field of light-activated cancer therapy has emerged,[2] in which optical fibers are used to deliver light for treatment of specific tissue regions.[3] Fiber optic components have been used to record electrical activity in cardiac tissue employing potential-sensitive dyes.[4,5] Moreover, simultaneous recordings of blood volume, oxygenation, and intracellular calcium levels have been made via optical fibers on the surface of the brain with a single indicator employing reflectance and fluorescence.[6] A particular advantage of fiber optic–based systems is that they provide a minimally invasive means of applying these techniques deep in tissue. Fiber optic probes have been used to record electrical activity at single[7,8] and multiple intramural sites in the intact heart.[9–12]

In order to interpret the data collected with optical fiber-based systems or to design appropriate fiber optic probes, information about fiber illumination and fluorescence collection volumes is required. For instance, action potential upstrokes obtained in cardiac tissue using optical mapping techniques are generally much slower than those in corresponding intracellular recordings.[12,13] This is not due to the response of the dyes employed. Optical potentials recorded from very small collection areas in isolated or confluent cell cultures[4,14] have upstroke velocities very similar to those measured intracellularly. It has been argued that the blurring of the upstroke is due to the spread of electrical activation through the region addressed by the imaging system.[13,15,16] On this basis, the capacity of a fluorescence imaging system to follow the activation upstroke should depend on propagation velocity and effective fluorescence collection volume.[13,15,16]

To date, no systematic study of the collection volumes of a range of fiber probes has been performed, and no one method for the determination of these volumes is widely accepted. Zhu and Yappert have presented a simple model for estimating the effective collection volumes of optical fibers[17] in nonabsorbing, nonscattering media. However, an experimental approach to this problem is more appropriate, particularly for biological tissues that exhibit complex absorption and scatter-

Address all correspondence to Bruce H. Smaill, The University of Auckland, Bioengineering Institute, Private Bag 92019, Auckland, New Zealand 1001; Tel: +64 9 373 7599 x 86302; Fax: +64 9 373 7499; E-mail: b.smaill@auckland.ac.nz

1083-3668/2007/12(3)/034033/12/$25.00 © 2007 SPIE

ing properties.[18,19] Byars et al. characterized the fluorescence collection volume of a 240-μm diam, multimode (MM) optical fiber in heart tissue,[10] but the approach employed had limited spatial resolution, and it is difficult to extrapolate from their findings to optical probes with different geometry.

The objective of the work described in this study was to characterize both illumination and fluorescence collection volumes in optical fibers of different diameters in nonscattering and scattering fluids and in tissue. Novel techniques utilizing two-photon (2P) microscopy and 2P flash photolysis have been developed for this purpose. In addition, a simple semi-empirical model of fluorescence collection for an optical fiber has been developed as a means of interpreting experimental data and to aid optical probe design.

2 Methods

2.1 *Definition of Effective Fluorescence Collection Volume*

The effective fluorescence detection volume for an optical fiber that is used to supply excitation light to, and collect fluorescent emission from, a region adjacent to its tip is determined by both its illumination and collection volumes. The illumination intensity distribution adjacent to the tip of a flat-cleaved fiber is assumed to be axisymmetric with respect to a cylindrical polar coordinate system (r,z), in which z is coincident with the axis of the fiber and the radial coordinate r is transverse to it. Following the analysis proposed by Zhu and Yappert,[17] the illumination efficiency is therefore represented as $I_e(r,z)$, where $0<I_e<1$, and the fluorescence collection efficiency is similarly represented as $I_c(r,z)$, where $0<I_c<1$. Provided that illumination intensities are sufficiently low to avoid saturation, the fluorescence signal (dF) collected from a small volume (dV), at location (r,z), can be expressed as:

$$dF(r,z) = \eta K C(r,z) I_c(r,z) I_e(r,z)\, dV, \tag{1}$$

where dV, the annular volume, is given by:

$$dV = 2\pi r\, \mathrm{d}r\, \mathrm{d}z, \tag{2}$$

and η and K are parameters proportional to the fluorescence quantum yield and absorptivity of the fluorophores, respectively, while $C(r,z)$ describes the concentration of fluorophore. $F(z)$, the total fluorescence signal collected from within a depth z, can be determined by integrating dF across that volume. In the following estimate, it is assumed that fluorophore distribution is constant:

$$F(z) = 2\pi\eta K C \int_0^z \int_0^\infty I_c(r,z) I_e(r,z) r\, \mathrm{d}r\, \mathrm{d}z. \tag{3}$$

Hence, the signal depends on the product of illumination and collection fields. The product

$$I_{eff}(r,z) = I_e(r,z) \times I_c(r,z), \tag{4}$$

describes the spatial properties of the fiber as a fluorescence probe and $I_{eff}(r,z)$ is defined as the effective collection field.

The relative fluorescence signal

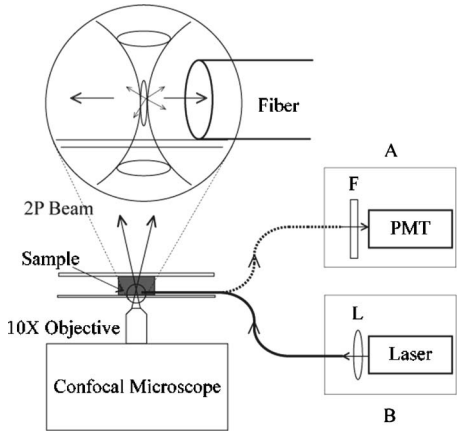

Fig. 1 Schematic diagram of the imaging system. The system consists of a 2P confocal microscope, a PMT with a selectable emission filter F and an external laser source. For two-photon excitation studies, the 2P laser in the confocal microscope was used to stimulate fluorophores in the focal volume adjacent to an optical fiber (see inset A), and fluorescent emission collected by the fiber was detected by the PMT. Laser scanning was used to reconstruct fluorescence collection fields. For flash photolysis measurements, the 2P laser in the confocal microscope was used to release caged fluorophores in the same focal volume. For studies of fiber illumination profiles, continuous illumination was routed through the fiber from the external laser source, and the time-course of fluorescent emission by the uncaged fluorophore was monitored by the confocal microscope. A similar flash photolysis approach was used to provide additional characterization of fiber collection profiles (see Sec. 2 for details).

$$R(z) = \frac{F(z)}{F(\infty)}, \tag{5}$$

specifies the fraction of total fluorescence collected within a distance z from the fiber tip.

2.2 *Measurement of Fluorescence Collection Fields*

Characterization of fiber response fields was performed by placing a fiber tip into the sample chamber (containing tissue or test solution) of a combined 2P/confocal laser scanning microscope (Zeiss LSM 410, Jena, Germany).[20] A mode-locked Titanium:Sapphire (Ti:S) laser (Mira 700, Coherent, Santa Clara, California) tuned to 750 nm provided excitation for 2P excitation of fluorophores or three-dimensionally resolved photorelease of caged fluoroscein. In the former cases, fluorescence emission was collected by the optical fiber under investigation, and measured with a photomultiplier tube (PMT) after passing through a bandpass emission filter (centered at 535 nm and 50-nm wide, Chroma, Brattleboro, Vermont), see Fig. 1. The microscope was used in 2P mode to create points of fluorescence emission by focusing the light of the Ti:S laser through a 10× objective into the sample. Since the fluorochrome concentration within the sample was uniform and the excitation profile resulting from 2P excitation was small compared to the length scale over which the collection field changed (i.e., it approximated a delta function), the fluorescence incident on the PMT was proportional to the value of $I_c(r,z)$ when the 2P excitation spot was placed at the coordinates (r,z) [see Eq. (3)]. In other words, the collection field was sampled by creating point sources of fluorescence of

constant intensity at specified locations. To reconstruct the axisymmetric collection field of a flat-cleaved fiber, it was sufficient to scan only in the plane containing the fiber axis. On the other hand, to characterize the asymmetric collection field of an angle-cleaved optrode,[9] it was necessary to collect a stack of such images.

The scan time for a single 512×512 (sampling resolution 2.5 μm) 2P image was typically 16 s, and the image signal-to-noise ratio (SNR) was improved by averaging over 16 images. For quantitative analysis, residual background was subtracted using control images recorded in the absence of 2P illumination.

2.2.1 *Measurement of collection fields with minimal fluorescence reabsorption*

Although the preceeding technique yielded data with good spatial resolution, it is possible that fluorescent emission from fluorophores experiences reabsorption by surrounding fluorophore. Therefore, a variation of the technique described earlier was used to determine I_C while minimizing attenuation of the fluorescence signal due to reabsorption by dye in the sample solution. A point source of fluorophore was provided by 2P excited flash photolysis of caged fluoroscein.[21] Short bursts (200-ms duration) of light from the Ti:S laser were focused into a sample containing 1.67 mM of caged fluoroscein using a 40×1.2 numerical aperture (NA) water immersion objective. The full-width half-maximum (FWHM) of the point spread function (PSF) of photorelease was ~ 0.5 μm in the x-y plane and 1.4 μm in the z-axis direction (coinciding with the axis of the objective).[20] The released fluorophore was excited through the same objective using 488-nm light from the argon ion laser in the confocal microscope, which was aligned confocal with the stationary photolysis spot. A more detailed account of these methods is given elsewhere.[20] During and after photolysis, the fluorescence received by the fiber was recorded while a line through the photolysis spot was repeatedly scanned with 488-nm light. For quantitative analysis, the line scan image was averaged temporally (50 ms, after termination of the 2P release flash) and spatially (over a 10-μm-wide region—see also Fig. 2) to obtain the collection efficiency at the photolysis spot. Due to diffusion, the full width of the fluorescence distribution at half maximal intensity was ~ 10 μm at the time of signal analysis (Fig. 2). While it was impractical to sample collection fields fully using 2P flash photolysis, this technique provides a means of characterizing their principal spatial features (see Sec. 3). The collection field adjacent to the fiber tip was characterized by performing 2P flash photolysis measurements at points 10 to 50 μm apart in the axial direction and at selected transverse distances from the fiber axis. Since the fluorochrome concentration was insignificant at sites other than the photolysis spot, fluorescence reabsorption within the sample was negligible.

2.3 *Determination of Illumination Fields*

Fiber illumination fields were also determined by utilizing 2P excited flash photolysis of caged fluoroscein. The illumination field for excitation of the released fluorophore was provided for the fiber under investigation by coupling the light from the 488-nm line of an argon ion laser (N57-796, Edmund Optics Singapore PTE Ltd.) into the fiber entrance (see Fig. 1). Fluorescence emission from fluoroscein released at the stationary 2P photolysis spot was measured through the microscope objective using one of the PMTs in the confocal microscope. The intensity of the fluorescence signal measured directly after release of the caged fluorophore (see Fig. 2) was thus proportional to the illumination efficiency of the fiber at the location of the photolysis spot. This follows from Eq. (1), since $C(r,z)$ was considered to be a delta function and the collection efficiency of the recording objective was constant. The illumination profile of the fiber was reconstructed from sequential intensity measurements at different sites along the plane containing the fiber axis.

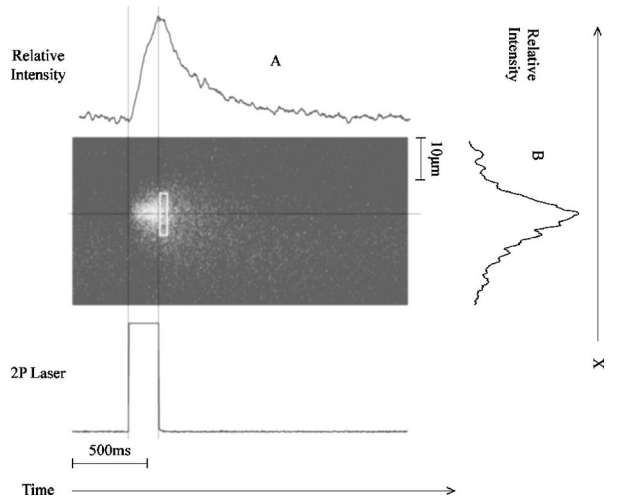

Fig. 2 Schematic diagram illustrating the flash photolysis technique. The 2P laser was used to release caged fluorophores in the focal volume adjacent to the fiber, which were then stimulated (see Fig. 1). Continuous line scans were acquired transverse to the fiber axis at this location. The 2P flash duration was 200 ms, and the time-course of fluorescent emission for a typical such recording is shown at the center of the figure. Fluorescent emission at the focal point is shown in (a) as function of time, while (b) is a line scan acquired at the termination of the 2P flash. The relative fluorescence intensity at the point addressed by the 2P flash is estimated by integrating across the 10 μm $\times 50$ ms space-time window indicated by the white rectangle (see Sec. 2 for further details). Note that the traces shown in (a) and (b) have been averaged to improve signal quality.

2.4 *Optical Fibers*

The detection volumes of several different optical fiber-types were characterized. The flat-cleaved fibers used were: a single-mode (SM) fiber with core diameter 4.0 μm and NA of 0.12 (FS-SN-3224, 3M), multimode (MM) graded index fibers with core diameters of 50 and 105 μm and NA of 0.22 (AFS50/125Y, AFS105/125Y, Thorlabs, Inc.), and an MM step-index fiber with core diameter 100 μm and NA of 0.22 (F-MCB-T, Newport Corp.). A more complex optical probe designed for multisite intratissue fluorescence mapping[9] was also characterized. This probe consists of angle-cleaved fibers (F-MCB-T, Newport Corp.) enclosed in a glass micropipette.

2.5 *Solution and Tissue Preparation*

The probes were characterized in both nonscattering and scattering solutions, as well as in stained tissue. Nonscattering solution containing 500 μM/L rhodamine was used for most

two-dimensional (2-D) confocal scanning studies, because the SNR was optimized at this fluorophore concentration. For flash photolysis studies, 1.67 mM/L of 10,000 MW 4,5-dimethoxy-2-nitrobenzyl (DMNB)-caged fluoroscein in dextran (Molecular Probes Corp.) were used. Scattering solutions were prepared by adding nonfluorescent 1-μm-diam microspheres at a concentration of 5.06×10^9 beads/mL to these aqueous solutions, resulting in scattering properties that mimic brain tissue.[22] In addition, 2-D confocal scanning studies were carried out for a flat-cleaved AFS105/125Y fiber in nonscattering solution at rhodamine concentrations ranging from 50 to 5000 μM/L to determine the effects of fluorophore concentration on fluorescence collection fields.

The tissue used in this study was taken from the hearts of 20-month-old Wistar Kyoto (WKY) rats. The rats were anaesthetized with halothane, decapitated, and the hearts were rapidly removed. Tissue slices (~1-mm thick) were cut from the free wall of the left ventricle (LV), oblique to the epicardial surface, and stained with rhodamine (1 mM/L) for 24 h at 4 °C. Subsequently, fiber optic probes were inserted manually into the section thickness and 2P excitation studies were carried out. All procedures were approved by the University of Auckland Animal Ethics Committee.

2.6 *Flux Distribution Model for Illumination Field*

One of the objectives of this study is to develop a model that can be used to estimate the illumination and effective fluorescence collection volumes in tissue for MM optical fibers of varying diameter and NA. In order to address this problem, we have set up a semiempirical model similar to that presented by Zhu and Yappert.[17]

The illumination intensity distribution at a given wavelength is represented as:

$$I_e(r,z) = E(r,z) \times D(z), \tag{6}$$

where energy loss is lumped in the axial decay component, $D(z)$ and $E(r,z)$ is a source term for which energy conservation applies. Thus, for all z

$$\int_0^\infty E(r,z) r \, dr = \text{constant}, \tag{7}$$

we assume that the decay is exponential and is expressed as:

$$D(z) = \exp(-\mu_t, z), \tag{8}$$

where the effective absorption coefficient, μ_t, is a wavelength-dependent space constant that reflects the loss of photons due to absorption and scattering of photons from within the measurement region.

The illumination source function $E(r,z)$ is the convolution of a simple Gaussian distribution $S_1(r,z)$, representing a single-mode illumination field, with a circular function $S_2(r,z)$ and is expressed as:

$$E(r,z) = S_1(r,z) *_r S_2(r,z), \tag{9}$$

where $*_r$ indicates that the convolution is performed only over the radial coordinate. The Gaussian function

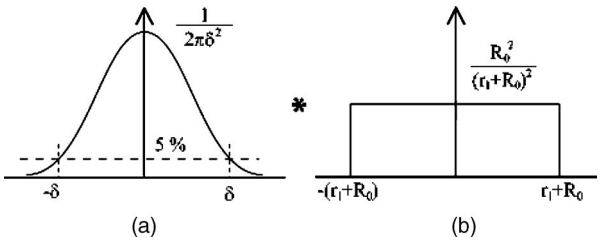

Fig. 3 Cross-sectional representations of the simple Gaussian function $S_1(r,z)$ and the spatial source term $S_2(r,z)$ that are convolved to form the illumination source function $E(r,z)$. Note that functions are normalized to ensure flux conservation.

$$S_1(r,z) = \frac{1}{2\pi\delta^2} \exp\left(-\frac{r^2}{2\delta^2}\right), \tag{10}$$

has a standard deviation δ that varies with z such that most of the light is contained within a cone defined by the NA of the fiber. Note that the boundaries set by the NA have a threshold level of 5% of the peak intensity as specified by the fiber manufacturer (see Fig. 3). Therefore, the standard deviation δ is defined as:

$$\delta = \left[\frac{(z\tan\theta)^2}{2\ln(0.05)}\right]^{\frac{1}{2}}, \tag{11}$$

where θ is determined from the NA of the fiber (NA) and the refractive index of the medium (n):

$$\theta = \sin^{-1}\left(\frac{NA}{n}\right). \tag{12}$$

The function $S_2(r,z)$ describes the circular area over which the Gaussian function $S_1(r,z)$ is convolved (in the radial coordinate) to generate the radial distribution of illumination at each axial position, and it incorporates a scale factor that ensures that energy is conserved as specified in Eq. (7).

$$S_2(r,z) = \begin{cases} \dfrac{R_0^2}{(r_1+R_0)^2}, & \text{if } r < r_1 + R_0, \\ 0, & \text{otherwise}, \end{cases} \tag{13}$$

where R_0 is the radius of the fiber and $r_1 = z\tan\theta_b$.

When $\theta_b = 0$, S_2 is independent of z and E corresponds to a distribution of essentially independent single modes originating at the face of the MM fiber. Under these circumstances, the predicted axial profile of the illumination intensity $E(r,z)$ is constant in the near-field, when the effective absorption coefficient $\mu_t = 0$. This does not match the fall in axial intensity in the near-field observed either in air or in nonscattering fluids (see Sec. 3), due, presumably, to redistribution of light in the radial direction that is not encompassed by the spread of a Gaussian function alone. To more closely match the fall of axial illumination in the near-field, we have allowed, as a first-order approximation, the radius of S_2 to vary linearly with z. Note that, in our simulations, θ_b is relatively small in comparison with θ.

A similar model should also describe the fluorescence collection efficiency at a given emission wavelength. However,

because fluorescent emission is distributed across a range of wavelengths, the fluorescent light collected from a point (r,z) will be affected by wavelength variation in both the intensity of emission and the decay component $D(z)$. To account for this, the collection efficiency I_c should be evaluated as follows:

$$I_c(r,z) = k\int_{\lambda_l}^{\lambda_u} E(r,z) \times F(\lambda) \times D(z,\lambda)\, d\lambda, \qquad (14)$$

where k is a scaling factor, and λ_u and λ_l are the upper and lower bounds, respectively, of the effective emission spectrum $F(\lambda)$ after filtering. It can be shown that this expression reduces to a form very similar to that in Eq. (6):

$$I_c(r,z) = E(r,z) \times D^*(z), \qquad (15)$$

where scaling constant and wavelength dependence are lumped in the weighted axial component $D^*(z)$.

This model has been used to interpret and analyze experimental data and to investigate systematically the effects of fiber diameter and NA on both illumination and effective fluorescence collection volumes. Effective fluorescence collection volumes are estimated as the product of illumination and fluorescence collection fields.

The model has also been used to study the extent to which a wave of altered fluorescence emission propagating through the volume addressed by a fiber will be blurred by varying contributions of regions within the collection field. This process is simulated by allowing a plane-wave impulse to propagate at various angles and propagation speeds through the effective collection field defined by the model. At any time, the fluorescence signal, $dF(r,z)$, is equal to the effective collection field [see Eq. (4)] along the impulse wavefront and is zero elsewhere. The total fluorescence signal was estimated by integrating across the entire volume as indicated in Eq. (3). This process was repeated sequentially to reconstruct the time-course of the optical signal collected as the plane-wave impulse moves across the volume addressed by the fiber.

3 Results

3.1 *Comparison of Illumination and Fluorescence Collection Profiles*

Flash photolysis was used to characterize illumination and collection fields under identical experimental conditions for a flat-cleaved fiber (F-MCB-T) in nonscattering and scattering media. Illumination and collection profiles mapped out along the fiber axis using 2P flash photolysis are superimposed in Fig. 4(a) on the axial collection profile measured in nonscattering rhodamine solution (100 μM/L) using 2P confocal microscopy. Note that these data were obtained with a 488-nm excitation source and that the fluorescence emission was collected at 535 nm. It is evident from Fig. 4(a) that there is no difference between axial illumination and collection profiles obtained with flash photolysis and that the axial collection data obtained with 2P confocal scanning in comparable conditions are consistent with these results.

The radial illumination profile in Fig. 4(b), measured with 2P flash photolysis, exhibits a flat top over the central region and decays toward the periphery, almost exactly matching the corresponding collection profile obtained with 2P confocal scanning with the same fiber in nonscattering fluid. Results observed in scattering fluids were also similar to those presented here. SNR was relatively low in these experiments. This was due to decreased signal levels, but traces of incompletely caged fluorophore also increased the background noise.

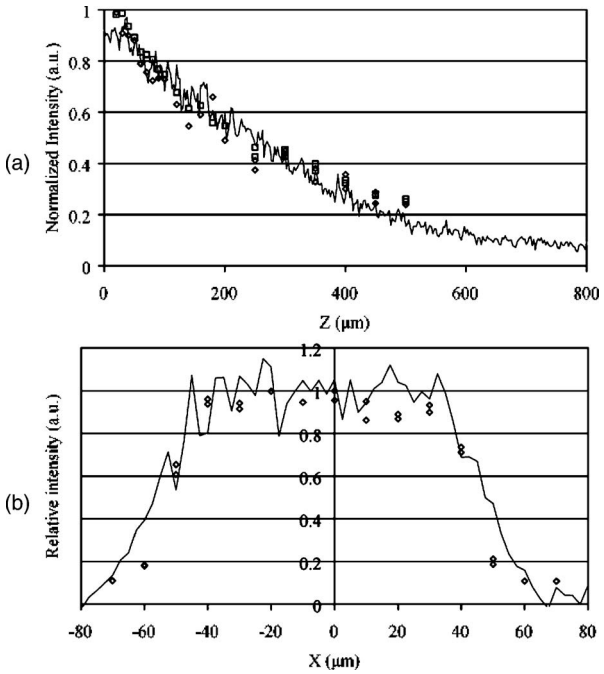

Fig. 4 Comparison of illumination and fluorescence collection profiles for an F-MCB-T optical fiber in nonscattering fluid. (a) Axial illumination and fluorescence collection measurements: illumination (□) and collection (◇) profiles obtained with 2P flash photolysis are compared with collection profile obtained with 2P confocal scanning (—). (b) Radial illumination and fluorescence collection measurements: illumination (□) profile obtained with 2P flash photolysis is compared with collection profile obtained with 2P confocal scanning (—) under comparable conditions.

3.2 *Fluorescence Collection Fields for Flat-Cleaved Optical Fibers*

Fluorescence collection fields of optical probes were measured with 2P confocal microscopy as described earlier. A typical 2-D collection field along the axis of an MM flat-cleaved fiber in nonscattering fluid is shown in Fig. 5(a). The axial intensity profile is shown in Fig. 5(b), while radial intensity profiles at z=50, 200, and 350 μm are superimposed in Fig. 5(c). The axial intensity falls progressively with distance from the fiber tip. However, the rate of axial decay appears to be less in the near-field than the far-field. The radial intensity distribution has a flat top adjacent to the tip of the fiber. This plateau is reduced as light spreads radially with increasing axial distance from the fiber tip. In the far-field, the radial intensity profile resembles a Gaussian distribution. The transition between these forms takes place around 250 μm from the fiber tip in this case, and in general, the axial distance at which this occurs is directly related to the fiber radius.

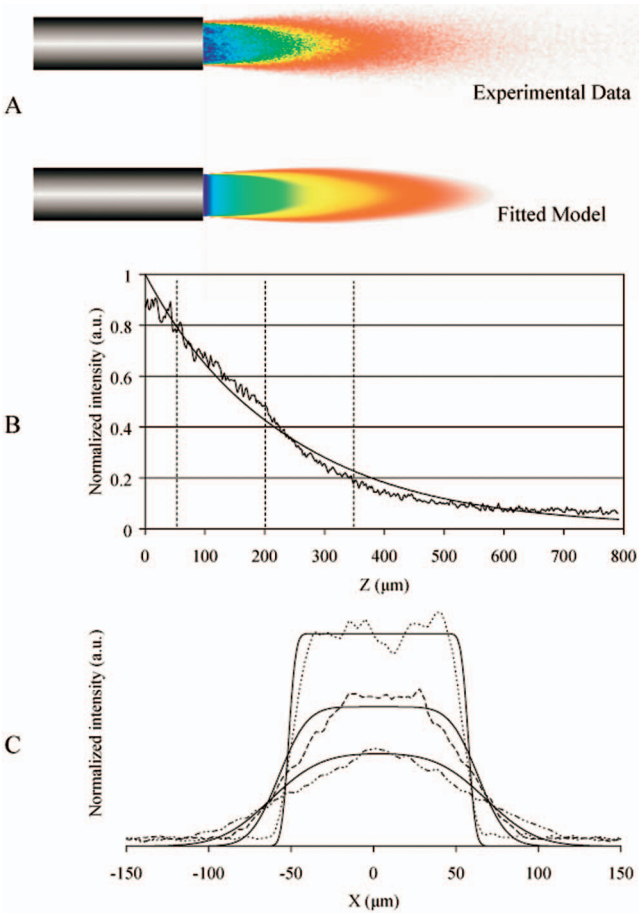

Fig. 5 Fluorescence collection field for an F-MCB-T optical fiber characterized using 2P excitation. (a) Measured 2-D intensity map and the corresponding model fitting. (b) Axial intensity profile. (c) Radial intensity profiles at axial locations indicated in (b) 50, 200, and 350 μm from the fiber tip. Note that results were obtained with nonscattering 500-μM/L rhodamine solution. The solid lines in (b) and (c) were fitted using the model.

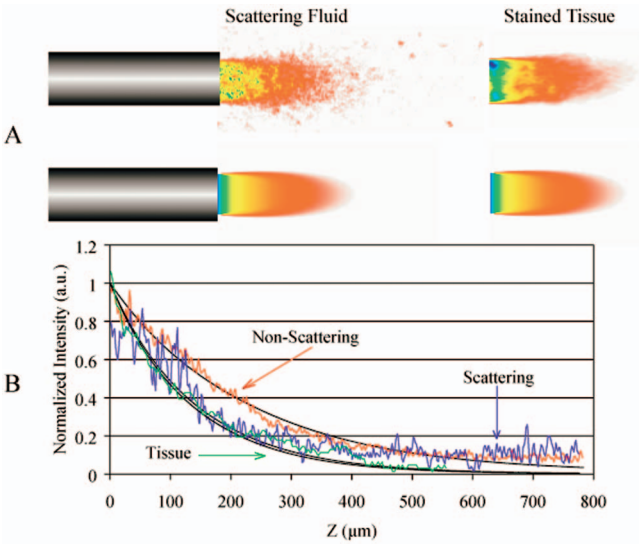

Fig. 6 Fluorescence collection field for an F-MCB-T optical fiber characterized using 2P excitation in different media. (a) 2-D intensity maps for scattering fluid and stained tissue and the corresponding model fittings. (b) Axial intensity profiles for tissue, nonscattering fluids, and scattering fluids. Note that results obtained with nonscattering and scattering fluids contained 500 μM/L rhodamine, while the tissue was stained with 1000 μM/L rhodamine. The solid lines in (b) are the corresponding fitting results using the model.

Typical collection fields for a MM fiber in scattering fluid and tissue are shown in Fig. 6(a). Corresponding axial intensity profiles in nonscattering and scattering fluids and in stained tissue are overlaid in Fig. 6(b). Note that the data here are smoothed using a moving average filter. There is significant attenuation of fluorescence collection intensity in scattering fluid and in tissue. However, the flat top of the radial intensity distribution adjacent to the fiber tip was preserved in all cases. It should be noted that the axial intensity profile in scattering medium exhibits considerably more decay than the corresponding profile in the nonscattering fluid.

3.3 *Model Validation*

The semiempirical model described in the Sec. 2 was validated by comparing predicted collection profiles with data obtained experimentally. Because fluorescent emission was collected across a relatively narrow wavelength window (535±25 nm), it was assumed that the weighted axial component $D^*(z)$ in Eq. (15) could be represented by a simple exponential expression as in Eq. (8). For a given MM fiber, the parameter θ_b that controls the spread of the function $S_2(r,z)$ [see Eq. (13)] was set as follows. Near-field axial intensity profiles observed in nonscattering fluid were matched to the model predictions by adjusting θ_b, having first estimated the effective absorption coefficient μ_t in this medium from measured photon loss. The effective absorption coefficient μ_t that best fit the model to experimental data was then determined for scattering fluid and tissue. For the AFS105/125Y fibers, this process was also carried out for nonscattering fluids at a series of rhodamine concentrations ranging from 50 to 1000 μM/L. Best-fit values for the effective absorption coefficient μ_t are given in Table 1.

Similar results were observed in the other flat-cleaved MM fibers tested. The average root-mean-square (RMS) error for the fit between the model and experimental data was 0.058±0.025 and 0.072±0.023 for axial and radial profiles, respectively. Background due to dark current was evident at low dye concentrations, but this was not subtracted from the experimental data.

3.4 *Quantification of Effective Collection Volumes*

The effective fluorescence collection efficiency I_{eff} is defined in Eq. (4) as the product of fluorescence collection and illumination efficiencies. Because illumination and fluorescence collection fields are very similar, I_{eff} can be approximated as the square of the measured collection efficiency distribution I_c and used to construct the relative fluorescence signal $R(z)$—see Eq. (5).

Figure 7 shows relative fluorescence signals for a flat-cleaved F-MCB-T fiber in nonscattering and scattering fluids and in tissue. The parameters Z_{50} and Z_{80}, which are defined as the axial depths at which R=50 and 80%, respectively, are used to quantify the effective collection volume of the fiber.

Table 1 Values of effective absorption coefficient that best fit model to experimental data. The average RMS error for the fit between model and data was 0.058±0.025 and 0.072±0.023, for axial and radial profiles, respectively. The parameter θ_b was set to 2 deg in all cases. The value indicated by * is the concentration of dye used to stain the tissue, not the actual dye concentration in the tissue.

Fiber diameter (μm)	Medium type	Dye concentration (μM/L)	Effective absorption coefficient, μ_t (mm^{-1})
50	Scattering fluid	500	3.4
50	Nonscattering fluid	500	1.7
100	Scattering fluid	500	3.4
100	Nonscattering fluid	500	1.6
100	Tissue	1000*	3.5
105	Scattering fluid	500	3.5
105	Nonscattering fluid	50	0.7
105	Nonscattering fluid	100	0.8
105	Nonscattering fluid	500	1.6
105	Nonscattering fluid	1000	2.2

Values for Z_{50} in stained tissue, scattering fluid, and nonscattering fluid are 75, 95, and 220 μm, respectively. Corresponding values of Z_{80} are 170, 195, and 465 μm.

Table 2 presents Z_{50} and Z_{80} for MM fibers of various diameters in nonscattering fluid. The radial FWHM of the effective collection profile at Z_{50} is also given. The results indicate that effective fluorescence collection volume of an MM fiber is directly related to its core diameter. While the data in Table 2 were acquired in nonscattering fluids at an emission wavelength of 535±25 nm, comparable results were also obtained in scattering fluid and at different emission frequencies. Z_{50} increased by less than 10% at 600 nm and was approximately halved in scattering fluid.

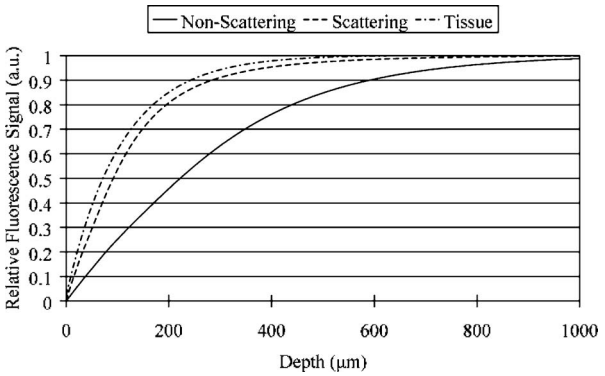

Fig. 7 Relative fluorescence signals for an F-MCB-T optical fiber in different media. Z_{50} in stained tissue, scattering fluids, and nonscattering fluids are 75, 90, and 220 μm, respectively. Corresponding values of Z_{80} are 175, 195, 90, and 465 μm. The fluorescence emission was measured at 535±25 nm.

Table 2 Effective collection dimensions for MM optical fibers of different diameter in nonscattering fluid at a rhodamine concentration of 500 μM/L. Note that fluorescence emission was measured at 535±25 nm.

Fiber Diameter (μm)	Medium type	Z_{50} (μm)	Z_{80}(μm)	FWHM at Z_{50} (μm)
50	Nonscattering fluid	125	240	40
100	Nonscattering fluid	220	465	95
105	Nonscattering fluid	240	550	100

3.5 *Effective Fluorescence Collection Volume of Purpose-Built Optical Probe (Optrode)*

The fluorescence collection profile of a purpose-built optical probe (optrode), in which hexagonally packed, angle-cleaved F-MCB-T fibers are enclosed in a glass micropipette, was also measured.

The fluorescence collection field in nonscattering fluid for a single optrode channel is presented in Fig. 8(a). The collection field is oriented radial to the probe axis and is more complex (and less symmetric) than for a flat-cleaved MM fiber. In Fig. 8(b), axial profiles for a single optrode channel in nonscattering fluid and tissue are compared with the profile in nonscattering fluid for a flat-cleaved F-MCB-T fiber. Effective collection dimensions for a single optrode channel were estimated from three-dimensional (3-D) two-photon excitation data. These results are given in Table 3.

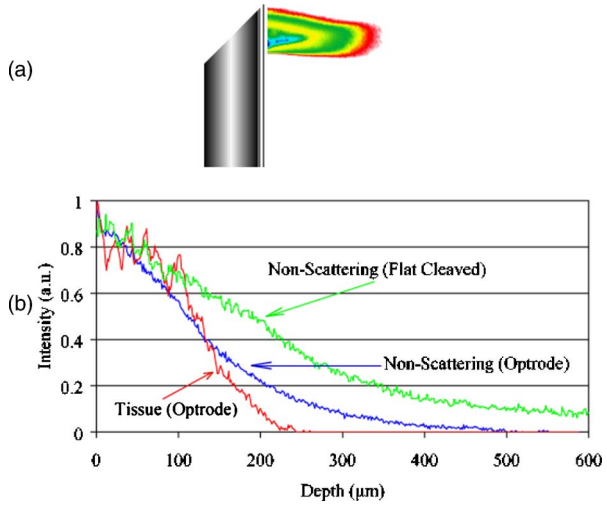

Fig. 8 Fluorescence collection field for a purpose-built fiber optic probe (optrode) characterized using 2P excitation. (a) 2-D intensity map in nonscattering fluid. (b) Axial intensity profiles for optrode in tissue and nonscattering fluid compared with profile for a flat-cleaved F-MCB-T optical fiber in nonscattering fluid. Note that the optrode is constructed from angle-cleaved F-MCB-T fibers (for further details see Sec. 2).

Table 3 Effective collection dimensions for a single optrode channel in nonscattering fluid and tissue.

Fiber type	Medium type	Z_{50} (μm)	Z_{80} (μm)	FWHM at Z_{50} (μm)
Optrode	Nonscattering fluid	105	230	65
Optrode	Tissue	72	152	60

3.6 *Effective Collection Volume and Propagated Impulse Response*

The volume from which fluorescence is collected determines the spatial resolution of functional fluorescence measurements. However, when propagating events such as calcium waves or electrical depolarization are being mapped, the time-course of the fluorescence signal may be blurred by the spread of the wave across the collection volume. To investigate this, we have simulated the temporal response of an impulse of fluorescence emission propagating as a plane-wave across optical fiber collection volumes of varying dimensions (see Sec. 2). The results of this study are presented in Fig. 9.

Figure 9(a) shows a simulated fluorescent signal propagating across a fiber collection volume at 0 deg, 45 deg, and 90 deg with respect to the fiber axis. Propagation across the collection volume broadens the fluorescent signal, and this blurring varies with impulse direction. The broadening is quantified by estimating the FWHM of the impulse response. FWHM is presented as a function of fiber diameter in Fig. 9(b) (Z_{50}=80 μm and propagation velocity=0.4 m/s) and as a function of Z_{50} in Fig. 9(c) (fiber diameter=100 μm and propagation velocity=0.4 m/s). Results for the propagation directions 0 deg and 90 deg are superimposed in both cases.

As expected, these results show that the blurring introduced by propagated fluorescent activity increases as the collection volume is enlarged. However, for a propagation velocity of 0.4 m/s (a velocity typical for spread of electrical excitation through cardiac tissue), the FWHM of the impulse response was less than 0.5 ms across the range of fiber diameters and Z_{50} values tested. Last, sensitivity to the direction of propagation depends on the effective collection dimensions. With a fiber diameter of 100 μm and Z_{50} equal to 80 μm, the effective collection volume is approximately isotropic, and the fact that the FWHM of the impulse response shown in Fig. 9(a) is not affected significantly by the propagation direction under these circumstances reflects this.

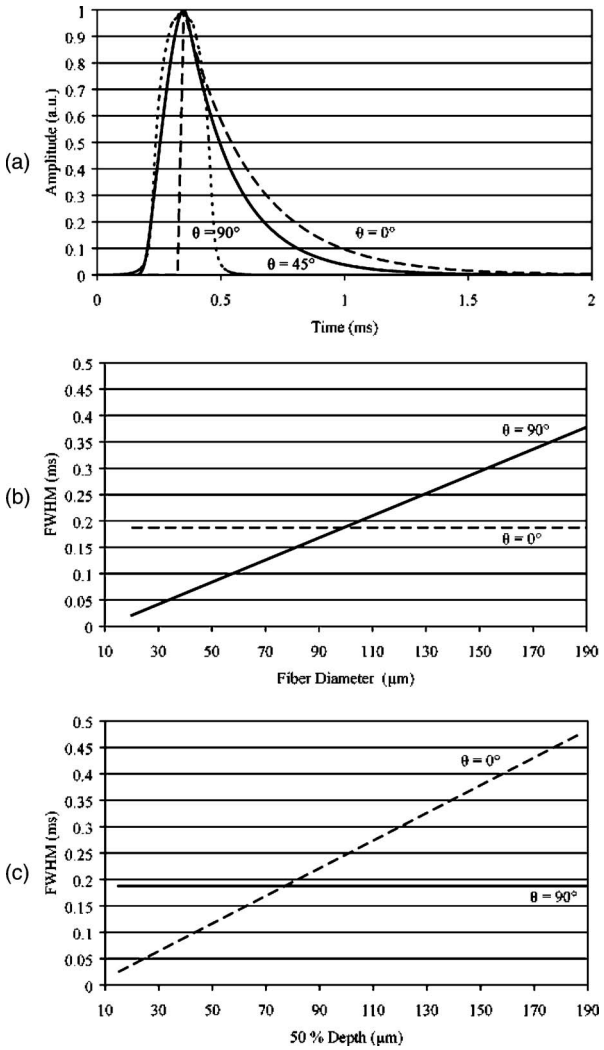

Fig. 9 Simulated fluorescent response of impulse propagating as a plane-wave across a fiber collection volume. (a) Impulse response for propagation at 0 deg, 45 deg, and 90 deg with respect to the fiber axis (Z_{50}=80 μm, fiber diam=100 μm, and propagation velocity =0.4 m/s). (b) FWHM of the impulse response as a function of fiber diameter (Z_{50}=80 μm and propagation velocity=0.4 m/s). (c) FWHM of the impulse response as a function of Z_{50} (fiber diam =100 μm and propagations velocity=0.4 m/s). Results for the propagation directions 0 deg and 90 deg are superimposed in both (b) and (c).

4 Discussion

The primary objective of this study was to identify both the illumination and fluorescence collection volumes of optical fibers in different fluid media, as well as in tissue. Systematic analyses were carried out with a variety of optical fibers employing novel methods that provide high spatial resolution. These include 2P excitation of rhodamine to measure fluorescence collection fields and 2P release of caged fluoroscein combined with confocal scanning microscopy to estimate illumination fields. Fluorescence collection fields have been characterized for flat-cleaved optical fibers and related to core diameter, NA, and optical properties (scattering and absorption) of the medium. We have also demonstrated that illumination and fluorescence collection profiles for MM fibers are essentially the same at comparable wavelengths. A semiempirical model was developed to describe the illumination and fluorescence collection fields for flat-cleaved MM fibers, and this has been used to interpret the experimental data. For an MM optical fiber with a core diameter of 100 μm and NA =0.22 in tissue, 80% of the total fluorescence in a wavelength window 535±25 nm excited by 488-nm illumination is collected from a volume that is approximately 170 μm deep and 105 μm in diameter. In conjunction with the model, these data provide a basis for designing fiber optic probes, with specific excitation and effective collection profiles. As far as

we are aware, this is the first time that illumination and collection profiles of optical fibers have been characterized systematically at high spatial resolution in a range of media, including soft tissue.

4.1 *Characterization of Illumination and Fluorescence Collection Fields*

The experimental techniques employed in this study to determine the illumination and fluorescence collection profiles incorporate a number of novel aspects that add to the precision of this study. First, 2P excitation illuminates an ellipsoidal volume that is small ($<1\%$) in comparison to the diameter of the optical fiber and can therefore be considered to be a point source. Because the 3-D location of the 2P focal volume can be precisely controlled, it is possible to reconstruct the fluorescence collection fields of optical fibers and fiber optical probes with high spatial resolution. Second, the 2P excitation wavelength (750 nm) is well separated from the spectral range of fluorescent emission for both rhodamine and fluorescein. Last, with 2P release of caged fluorophores, it is possible to sample fiber illumination profiles in a fashion similar to that used to characterize fluorescence collection fields. Moreover, the use of flash photolysis also means that confounding effects of light absorption by the fluorophore are minimized, since caged fluorophores outside the region addressed by the 2P focal volume do not respond to excitation. In any case, this study demonstrates that the three-dimensionally resolved nature of 2P excitation allows accurate characterization of illumination and collection fields of arbitrary probes or other optical elements as long as the fields are moderately larger than achievable 2P point spread functions (<1 μm).

The ellipsoidal shape of the 2P focal spot may affect the resolution with which illumination and fluorescence collection volumes can be characterized experimentally. With a $40\times$ 0.9 NA objective, the FWHM of the 2P focal volume was 0.5 μm in the x-y plane but 1.4 μm in the z-axis direction, and for lower magnification objectives, where NA is reduced, elongation in the z direction was proportionately worse. This has little impact on the axially symmetric illumination and fluorescence collection fields associated with the individual optical fibers studied here. In this case, it can be shown that the x-y resolution of the objective applies, except in the near-field. No significant differences were observed between images obtained with the $10\times$ and a $40\times$ objective, and we therefore used a $10\times$ objective since it covered a significantly larger field of view. However, the spread of the 2P focal volume in the z direction does give rise to signal blurring when characterizing illumination and collection fields that are not axially symmetric. The resultant degradation of resolution can always be overcome by using high NA objectives and employing image tiling to cover the required field of view.

4.2 *Effective Collection Volume*

The fact that measured illumination and fluorescence collection fields for flat-cleaved MM fibers were very similar in both nonscattering and scattering fluids is noteworthy. Absorption and scattering are wavelength-dependent, and the wavelengths of excitation light and fluorescent emission are different. In this study, however, fluorescence was collected over a relatively narrow wavelength window close to the excitation wavelength. Moreover, we have shown that collection volumes are strongly determined by scattering, which is more weakly dependent on wavelength than absorption (see the following discussion). Within this context, it is not surprising that the techniques employed could not resolve differences between illumination and collection volumes. We have also independently reconstructed the 3-D illumination field of an optical fiber in air by imaging light intensity scattered from a thin film transverse to it at a series of different axial locations. A confocal microscope in wide-field mode was used for this purpose. The results (not shown) match the detailed fluorescence collection fields obtained with 2P excitation when absorption and scattering are minimized. These results provide objective justification for the reconstruction of effective fluorescence collection volumes from measured fluorescence collection fields using the relationship [see Eq. (1)]:

$$dF(r,z) = \eta K I_c(r,z)^2 \, dV. \tag{16}$$

4.3 *Comparison with Previous Work*

A number of studies of effective fluorescence collection dimensions have been published.[7,9,10,13,15,23–26] The effect of the propagation of cardiac electrical activation across the effective collection volume on measured optical potentials has also been considered,[13,15,25,26] with reported collection depths in tissue ranging from $\sim$100 μm (Ref. 9) to $>$1 mm (Ref. 25). In part, this variance reflects the different means of fluorescence excitation and collection used. Focusing on previous results that are most comparable with ours, Krauthamer et al.[7] measured illumination intensity profiles for SM and MM optical fibers in air but report significantly greater axial attenuation than we do and observed no significant effect of fiber diameter on collection depth. Like us, Byars et al.[10] characterized the effective collection volumes of MM optical fibers in cardiac tissue. Their results for a flat-cleaved fiber with core diameter 240 μm and NA 0.51 are consistent with a value of Z_{50} around 800 μm, while we would expect Z_{50} to be less than 300 μm for an optical fiber with these specifications in tissue. Byars et al. characterized axial attenuation by passing a fiber through an excised LV wall segment from the endocardial surface until it touched a layer of absorbent paper soaked with fluorophore attached to the epicardial surface. Measurements were then made at a number of points through the LV as the fiber was withdrawn. We note that their axial steps were very coarse (500 μm), and it is unknown to what extent the optical properties of tissue might have been affected by the track previously made by the fiber.

Ding et al.[24] used Monte Carlo simulations to investigate the effects of illumination and collection diameters on effective collection depth. Their predicted Z_{50} for illumination and collection diameters of 100 μm was around 200 μm, which closely matches our results with optical fibers of comparable dimension. Hooks[9,27] measured effective collection volumes for flat-cleaved MM optical fibers in nonscattering fluid by recording the fluorescence collected as the fiber was moved toward the edge of a cuvette containing dye solution. The results—Z_{50} was 140 μm and 224 μm, respectively, for MM optical fibers with core diameters of 65 μm and 100 μm—are very similar to those given here. Knisley et al.[23] employed a similar approach to estimate effective fluores-

cence collection depths in cardiac tissue. They used a 100-μm laser beam to excite regions of different tissue thickness along a wedge of LV myocardium stained with di-4-ANEPPS and stated that the thickness of tissue contributing to fluorescence was around 300 μm. In comparison, the Z_{80} reported here for a 100-μm MM fiber is 170 μm. This difference is due to the fact that Knisley et al. collected fluorescence emission with a PMT, which has a much larger detection area than the optical fiber used in our case. When the effects of collection dimension are accounted for using the theoretical analysis outlined earlier,[24] their results are entirely consistent with ours.

4.4 *Validation of the Model*

The model outlined in this paper provides a semiempirical description of the illumination field adjacent to the tip of a flat-cleaved MM fiber. The approach employed has a number of similarities to a model previously presented by Zhu and Yappert.[17] These investigators represented the distribution of light radial to the fiber axis as a Gaussian function with a standard deviation that was a linear function of axial position. As in our model, losses due to absorption and scattering were lumped as a single axial exponential decay. Such a model could not account for the complexity of the illumination field observed near the tip of an MM fiber, and Zhu and Yappert[17] acknowledged that "for multi-mode fibers a multi-Gaussian distribution should be used." In our model, we have constructed such a distribution by convolving a Gaussian function (representing single-mode propagation) with a circular source area transverse to the fiber axis. The diameter of the radial distribution source is identical to that of the fiber core at its tip but is also a linear function of axial position, which enabled us to accommodate redistribution of light in the radial direction that is not encompassed by the spread of a Gaussian function alone.

The model provided a good fit to the fluorescence collection fields measured using 2P excitation and fit the 2P flash photolysis data equally well. The radial distribution function accurately represented experimental intensity profiles transverse to the fiber axis in near- and far-fields. In particular, it reproduced the flat-topped radial intensity distribution adjacent to the fiber tip and the Gaussian distribution distant from it. It also predicted the axial distance at which the transition between these two profiles was observed. However, when μ_t was low, there were small but systematic differences between observed and predicted axial intensity profiles. Under these circumstances, the rate of axial attenuation was slightly less in the near-field than in the far-field, but this is not completely matched by the model [see Fig. 5(b)]. Residual asymmetries that are probably the result of modal fluctuation,[28–30] and are most evident in radial intensity profiles, also cannot be reproduced by the model [see Fig. 5(c)]. For individual model fits, however, the RMS error was on the order of the regional variation introduced by modal fluctuation and optical scattering. Taken together, these observations confirm the robustness of the model.

4.5 *Scattering and Absorption*

Tissue exhibits marked scattering of light and weaker frequency-dependent light absorption. Optical scattering is a complex process, and this is reflected by the fluorescence collection profiles presented in Fig. 6 for a flat-cleaved fiber (F-MCB-T) in scattering fluid and stained tissue. There is much greater regional variability in the fluorescence collection field for the scattering fluid [see Fig. 6(a)] than in equivalent results for a nonscattering fluid [see Fig. 5(a)]. It is also evident from these figures that fluorescent light originating from outside the NA of the fiber has a higher probability of being collected in the scattering fluid than in the nonscattering fluid. The scattering fluids prepared for this study provide an isotropic scattering environment,[22] whereas scattering in tissue is generally highly anisotropic. For the data shown in Fig. 6(a), at least, there appears to be greater regional variability for the stained tissue than for scattering fluid.

Despite the complexity of these processes, it has been suggested that optical scattering can be treated as an isotropic "absorption-like" event, provided that the dimensions of the volume of interest are greater than the scattering mean-free-path length.[17,19] According to Patterson and Pogue,[19] the mean-free-path-length in biological tissues is 71 μm at 500 nm. On this basis, scattering was lumped with absorption as a single axial decay term in our model. While scattering markedly affects fluorescence collection characteristics and gives rise to substantial regional variability (Fig. 6), the model nonetheless provides a good estimate of the average intensity distribution. This validates the assumption that optical scattering in large volumes can be approximated as isotropic absorption.

While it is difficult to quantify actual fluorophore concentration in stained tissue, dye absorption will likely reduce effective collection volumes for such membrane potential sensitive dyes as di-4-ANNEPS, which is typically administered at relatively high concentrations.[12] Effective collection volume is therefore reduced at high fluorophore concentrations, but this can be ignored at concentrations $<\sim 100$ μM/L. Ding et al. have measured the optical properties of di-4-ANEPPS stained rabbit heart and report values for absorption μ_a and scattering μ_s of 0.52 ± 0.13 mm^{-1} and 23.0 ± 2.5 mm^{-1}, respectively, at 488 nm. Corresponding values at 669 nm were $\mu_a=0.10\pm0.04$ mm^{-1} and $\mu_s=21.8\pm2.5$ mm^{-1} (Ref. 24). Our estimates of total absorption for cardiac tissue were 3.5 mm^{-1}, which is much larger than the value for absorption μ_a quoted earlier, but significantly less than quoted scattering coefficients indicating that some scattered light is collected by the fiber optic probe. This suggests that scattering plays an important role in the axial decay of effective fluorescence collection efficiency for fiber optic probes in tissue. This view is reinforced by the observation that very similar estimates of total absorption were made for probes in scattering fluid at the same dye concentration.

4.6 *Determinants of Effective Fluorescence Collection Volumes in Fiber Optic Probes*

The experiments and modeling studies reported here demonstrate that the dimensions of the effective fluorescence collection volume for a flat-cleaved optical fiber are mainly determined by its core diameter and by the optical properties of the medium in which it is used. We have shown that a change in fiber diameter from 50 to 100 μm gives rise to changes of similar magnitude in collection volume dimensions (see Table

1). However, we found that the influence of fiber diameter on effective collection volume was reduced when the axial decay constant was high, for instance, in cardiac tissue. These experimental observations are matched by the model, which also predicts similar trends when the fiber diameter is increased from 100 to 200 μm. While the effect of altering NA was not considered experimentally, the model predicts a relatively modest reduction in Z_{50} when NA is doubled—less than 10% in a nonscattering fluid and less still in scattering fluids and tissue.

The fluorescence collection field of a purpose-built fiber optic probe (optrode) that consists of multiple angle-cleaved MM fibers enclosed in a glass micropipette[9] was similar in shape but significantly smaller. We ascribe these differences to lensing effects as light passes through the curved surface of the fiber and also to scattering at interfaces in the probe, where there is a refractive index mismatch.

4.7 *Effects of Propagation on Fluorescence Impulse Response of Optical Probes*

It has been noted previously that the upstroke of the cardiac action potential observed in optical recordings is generally much slower than rapid depolarization in corresponding intracellular measurements.[12,13] This has been attributed to the spread of electrical activation through the region addressed by the imaging system.[13,15,16,31,32] According to our analysis, propagation at 0.4 m/s produces blurring of the impulse response that is dependent on the direction of propagation and the dimensions of the effective collection volume. However, the FWHM for the impulse response in tissue was less than 0.5 ms for an optical fiber with a core diameter of 100 μm and Z_{50} of 80 μm, regardless of propagation direction. It is noteworthy that directional sensitivity of fiber optic probes is minimized when the collection volume is relatively isotropic. However, it would be possible to design probes with specific directional sensitivity on the basis of the information provided in this paper. Electrical activation propagates through a normal ventricular myocardium at 0.2 to 1 m/s (Refs. 33–35), and rise-times of ventricular action potentials recorded using fiber optic probes with core diameters of 100 μm range from 5 to 10 ms (Refs. 7, 9, and 10). Less than 1 ms of this upstroke time can be explained by the spread of activation across the relatively small collection volume of these probes. This discrepancy is perplexing and should be subjected to more-detailed investigation in the future.

4.8 *Limitations of the Study*

There are some obvious limitations to the results presented in this study, and these will now be discussed. First, the optical fibers tested all had the same NA. While the model suggests that NA has a limited affect on Z_{50} in tissue, this prediction has yet to be tested experimentally. Second, the experimental results presented here were obtained at a limited number of wavelengths. A variety of excitation wavelengths are used with functional fluorescence recordings, and emission spectra for most fluorophores occupy a relatively broad range of wavelengths. In addition, the absorption of light in tissue is strongly frequency dependent, whereas scattering is much less so.[18,19] However, we have demonstrated that effective collection volumes in tissue are dominated by scattering for fiber optic imaging systems (although this is less so for systems with larger collection dimensions). We have also shown that the variation of μ_t with wavelength is relatively small, and should therefore be possible to account for using a simple linear correction. A further difficulty is that estimates of μ_t at low dye concentrations are based on fluorescence recordings with low SNR. The reliability of the absolute μ_t values presented here may therefore be limited by confounding effects of dark-noise. Last, while the model used in this study was useful and relatively robust, it is nonetheless semiempirical. To represent illumination and fluorescence collection fields more completely, it will be necessary to use a representation that is based firmly on the fundamental principles of physical optics.

5 Conclusions

In this study, we have used powerful new techniques to characterize the illumination and fluorescence collection volumes of optical fibers at much higher spatial resolution than previously reported. Systematic analyses were carried out with a variety of fiber optic probes in tissue and different fluid media. In addition, a semiempirical model was developed to describe the illumination and fluorescence collection fields for flat-cleaved optical fibers. This has been used to interpret the experimental data and also provides a foundation for the design of fiber optic probes. On the basis of this work, we have developed a firm understanding of the way in which fiber geometry, absorption, and scattering of light in the medium determine effective fluorescence collection fields and time resolution in propagation measurements.

Acknowledgments

This work was funded by the New Zealand Marsden Fund and by the Health Research Council of New Zealand. Dean Tai was supported by a University of Auckland Doctoral Scholarship and was also a recipient of a Richard Bates Memorial Scholarship from the Royal Society of New Zealand.

References

1. Y. Chen, G. Zheng, Z. H. Zhang, D. Blessington, M. Zhang, H. Li, Q. Liu, L. Zhou, X. Intes, S. Achilefu, and B. Chance, "Metabolism-enhanced tumor localization by fluorescence imaging: *in vivo* animal studies," *Opt. Lett.* **28**, 2070–2072 (2003).
2. R. Ackroyd, C. Kelty, N. Brown, and M. Reed, "The history of photodetection and photodynamic therapy," *Photochem. Photobiol.* **74**, 656–669 (2001).
3. F. Gad, T. Zahra, K. P. Francis, T. Hasan, and M. R. Hamblin, "Targeted photodynamic therapy of established soft-tissue infections in mice," *Photochem. Photobiol. Sci.* **3**, 451–458 (2004).
4. S. Rohr and J. P. Kucera, "Optical recording system based on a fiber optic image conduit: assessment of microscopic activation patterns in cardiac tissue," *Biophys. J.* **75**, 1062–1075 (1998).
5. I. R. Efimov, V. P. Nikolski, and G. Salama, "Optical imaging of the heart," *Circ. Res.* **95**, 21–33 (2004).
6. C. Du, A. P. Koretsky, I. Izrailtyan, and H. Benveniste, "Simultaneous detection of blood volume, oxygenation, and intracellular calcium changes during cerebral ischemia and reperfusion *in vivo* using diffuse reflectance and fluorescence," *J. Cereb. Blood Flow Metab.* **25**, 1078–1092 (2005).
7. V. Krauthamer, H. J. Bryant, C. C. Davis, and T. W. Athey, "Action potential-induced fluorescence changes resolved with an optical fiber carrying excitation light," *J. Fluoresc.* **1**, 207–213 (1991).
8. M. Neunlist, S. Z. Zou, and L. Tung, "Design and use of an optrode for optical recordings of cardiac action-potentials," *Pfluegers Arch.* **420**, 611–617 (1992).

9. D. A. Hooks, I. J. LeGrice, J. D. Harvey, and B. H. Smaill, "Intramural multisite recording of transmembrane potential in the heart," *Biophys. J.* **81**, 2671–2680 (2001).
10. J. L. Byars, W. M. Smith, R. E. Ideker, and V. G. Fast, "Development of an optrode for intramural multisite optical recording of V_m in the heart," *J. Cardiovasc. Electrophysiol.* **14**, 1196–1202 (2003).
11. D. C. S. Tai, B. J. Caldwell, I. J. LeGrice, D. A. Hooks, A. J. Pullan, and B. H. Smaill, "Correction of motion artifact in transmembrane voltage-sensitive fluorescent dye emission in hearts," *Am. J. Physiol. Heart Circ. Physiol.* **287**, H985–H993 (2004).
12. B. J. Caldwell, I. J. LeGrice, D. A. Hooks, D. C. S. Tai, A. J. Pullan, and B. H. Smaill, "Intramural measurement of transmembrane potential in the isolated pig heart: validation of a novel technique," *J. Cardiovasc. Electrophysiol.* **16**, 1001–1010 (2005).
13. S. D. Girouard, K. R. Laurita, and D. S. Rosenbaum, "Unique properties of cardiac action potentials recorded with voltage-sensitive dyes," *J. Cardiovasc. Electrophysiol.* **7**, 1024–1038 (1996).
14. D. K. L. Cheng, L. Tung, and E. A. Sobie, "Nonuniform responses of transmembrane potential during electric field stimulation of single cardiac cells," *Am. J. Physiol. Heart Circ. Physiol.* **277**, H351–H362 (1999).
15. C. J. Hyatt, S. F. Mironov, M. Wellner, O. Berenfeld, A. K. Popp, D. A. Weitz, J. Jalife, and A. M. Pertsov, "Synthesis of voltage-sensitive fluorescence signals from three-dimensional myocardial activation patterns," *Biophys. J.* **85**, 2673–2683 (2003).
16. D. L. Janks and B. J. Roth, "Averaging over depth during optical mapping of unipolar stimulation," *IEEE Trans. Biomed. Eng.* **49**, 1051–1054 (2002).
17. Z. Y. Zhu and M. C. Yappert, "Determination of effective depth and equivalent pathlength for a single-fiber fluorometric sensor," *Appl. Spectrosc.* **46**, 912–918 (1992).
18. W. F. Cheong, S. A. Prahl, and A. J. Welch, "A review of the optical properties of biological tissues," *IEEE J. Quantum Electron.* **26**, 2166–2185 (1990).
19. M. S. Patterson and B. W. Pogue, "Mathematical model for time-resolved and frequency-domain fluorescence spectroscopy in biological tissues," *Appl. Opt.* **33**, 1963–1974 (1994).
20. C. Soeller and M. B. Cannell, "Construction of a two-photon microscope and optimisation of illumination pulse duration," *Pfluegers Arch.* **432**, 555–561 (1996).
21. M. B. Cannell, M. D. Jacobs, P. J. Donaldson, and C. Soeller, "Probing microscopic diffusion by 2-photon flash photolysis: measurement of isotropic and anisotropic diffusion in lens fiber cells," *Microsc. Res. Tech.* **63**, 50–57 (2004).
22. P. Theer, M. T. Hasan, and W. Denk, "Two-photon imaging to a depth of 1000 μm in living brains by use of a $Ti:Al_2O_3$ regenerative amplifier," *Opt. Lett.* **28**, 1022–1024 (2003).
23. S. B. Knisley, "Transmembrane voltage changes during unipolar stimulation of rabbit ventricle," *Circ. Res.* **77**, 1229–1239 (1995).
24. L. Ding, R. Splinter, and S. B. Knisley, "Quantifying spatial localization of optical mapping using Monte Carlo simulations," *IEEE Trans. Biomed. Eng.* **48**, 1098–1107 (2001).
25. W. T. Baxter, S. F. Mironov, A. V. Zaitsev, J. Jalife, and A. M. Pertsov, "Visualizing excitation waves inside cardiac muscle using transillumination," *Biophys. J.* **80**, 516–530 (2001).
26. C. J. Hyatt, S. F. Mironov, F. J. Vetter, C. W. Zemlin, and A. M. Pertsov, "Optical action potential upstroke morphology reveals near-surface transmural propagation direction," *Circ. Res.* **97**, 277–284 (2005).
27. D. A. Hooks, "Three-dimensional mapping of electrical propagation in the heart: experimental and mathematical model based analysis," PhD Thesis, Univ. of Auckland (2002).
28. D. B. S. Soh, J. Nilsson, S. Baek, C. Codemard, Y. C. Jeong, and V. Philippov, "Modal power decomposition of beam intensity profiles into linearly polarized modes of multimode optical fibers," *J. Opt. Soc. Am. A* **21**, 1241–1250 (2004).
29. R. Rokitski and S. Fainman, "Propagation of ultrashort pulses in multimode fiber in space and time," *Opt. Express* **11**, 1497–1502 (2003).
30. V. Doya, O. Legrand, F. Mortessagne, and C. Miniatura, "Speckle statistics in a chaotic multimode fiber," *Phys. Rev. E* **65**, 056223 (2002).
31. S. F. Mironov, F. J. Vetter, and A. M. Pertsov, "Fluorescence imaging of cardiac propagation: spectral properties and filtering of optical action potentials," *Am. J. Physiol. Heart Circ. Physiol.* **291**, H327–H335 (2006).
32. M. J. Bishop, B. Rodriguez, J. Eason, J. P. Whiteley, N. Trayanova, and D. J. Gavaghan, "Synthesis of voltage-sensitive optical signals: application to panoramic optical mapping," *Biophys. J.* **90**, 2938–2945 (2006).
33. B. G. D. Duker, "Frequency-dependent effects of tocainide, quinidine, and flecainide on conduction as reflected in the rise time of the monophasic action-potential in the isolated guinea-pig heart," *Cardiovasc. Res.* **25**, 217–222 (1991).
34. M. D. Halbach, U. Egert, J. Hescheler, and K. Banach, "Estimation of action potential changes from field potential recordings in multicellular mouse cardiac myocyte cultures," *Cell. Physiol. Biochem.* **13**, 271–284 (2003).
35. A. O. Verkerk, M. W. Veldkamp, F. Abbate, G. Antoons, L. N. Bouman, J. H. Ravesloot, and A. C. G. van Ginneken, "Two types of action potential configuration in single cardiac Purkinje cells of sheep," *Am. J. Physiol. Heart Circ. Physiol.* **277**, H1299–H1310 (1999).